Contents lists available at ScienceDirect

Thin-Walled Structures

journal homepage: www.elsevier.com

Full length article

Comparative study of stirrup-confined circular concrete-filled steel tubular stub columns under axial loading

Fa-xing Ding[a, d], Jiang Zhu[a], ShanShan Cheng[b, *], Xuemei Liu[c]

[a] School of Civil Engineering, Central South University, Changsha, Hunan Province 410075, PR China
[b] School of Engineering, University of Plymouth, Plymouth PL4 8AA, United Kingdom
[c] School of Civil Engineering and Built Environment, Queensland University of Technology, Brisbane, QLD 4001, Australia
[d] National Engineering Laboratory for High Speed Railway Construction, Changsha 410075, PR China

ARTICLE INFO

Keywords:
Circular CFT stub columns
Stirrup-confinement
Comparative study
Composite action
Ultimate bearing capacity

ABSTRACT

This paper presents a comparative study of circular concrete-filled steel tubular stub columns with three different stirrup confinement types: bidirectional stirrups, loop stirrups and orthogonal stirrups. Axial compression tests have been carried out aiming at investigating the effects of the stirrup form and volume-stirrup ratio on the mechanical behavior of the stirrup-confined circular CFT stub columns, and ABAQUS was used to carry out the 3D numerical modelling. Radial stress of the core concrete and the composite action among the steel tube, stirrups and the core concrete have been investigated. It is found that the confinement provided by stirrups on core concrete strongly outperforms that provided by steel tube, steel sections or steel reinforcement. Furthermore, a simplified approach was developed to predict the ultimate bearing capacity of stirrup-confined circular CFT stub columns, which agreed well with the experimental and numerical results.

Nomenclature

A_c	Cross-sectional area of the core concrete
A_s	Cross-sectional area of the steel tube
A_{sso}	The converted cross-sectional area of the stirrup
A_{sc}	Total area of cross-section
d	Diameter of the stirrup
D	Diameter of the circular section
f_c	Uniaxial compressive strength of concrete
f_{cu}	Compressive cubic strength of concrete
f_s	Yield strength of the steel tube
f_{sv}	Yield strength of stirrups
f_{sc}	Ultimate strength of CFT column
k	Lateral pressure coefficient
L	Height of specimens
N_u	Axial ultimate bearing capacity of stirrup-confined circular CFT stub columns
$N_{u,3}$	Ultimate bearing capacity of stirrup-confined circular CFT stub columns
$N_{u,e}$	Ultimate bearing capacity of stirrup-confined circular CFT stub columns from test results
$N_{u,fe}$	Ultimate bearing capacity of stirrup-confined circular CFT stub columns from FE results
t	Wall thickness of the steel tube
σ	Axial stress of concrete
σ_i	Equivalent stress of steel tube
$\sigma_{L,s}$	Axial compressive stress of steel tube
$\sigma_{r,c}$	Radial concrete stress of the confined area
$\sigma_{r,cr}$	radial stress of core concrete caused by stirrups
$\sigma_{\theta,s}$	Tensile transverse stress of steel tube
ε	Axial strain of concrete
ε_c	Strain corresponding with the peak compressive stress of concrete
ε_L	Axial strain of columns
ε_i	Equivalent strain of steel tube
ε_y	Yield strain of the steel tube
ν_{sc}	Poisson's ratio of steel tube
ρ_s	Steel ratio of the steel tube
ρ_{sv}	Volume-stirrup ratio
ρ_{sa}	Equivalent stirrup ratio

* Corresponding author.
Email address: shanshan.cheng@plymouth.ac.uk (S. Cheng)

https://doi.org/10.1016/j.tws.2017.11.033
Received 21 June 2017; Received in revised form 11 November 2017; Accepted 16 November 2017
Available online xxx
0263-8231/

ρ_{so}	Overall steel ratio

1. Introduction

Concrete-filled steel tubular (CFT) columns have been widely used in high-rise/super-high-rise buildings, urban bridges and large-span structures, thanks to their excellent static and earthquake-resistant capacities. Circular tube shows best confinement to the core concrete of CFT columns. However, the thickness of the steel tube is limited due to weldability and construction concerns for large-diameter CFT columns [1]. In order to improve the mechanical performance of CFT columns without increasing the wall thickness of the steel tube, various methods have been proposed. Regarding the existing concrete-filled steel tubular columns, FRP strengthening methods (by wrapping the steel tube with FRP materials) have been comprehensively studied in [2–5]. FRP could generally help resist local buckling and improve ultimate bearing capacity of columns significantly, but the ductility may be decreased due to FRP rupture and sudden deterioration at the ultimate state. On the other hand, for newly built CFT columns, the methods of adding steel inside the steel tube have been extensively used to improve the overall steel ratio and ultimate capacity of the CFT stub column. For example, Hassanein et al. [6,7] studied the mechanical behavior of double skin tubular short columns, and found that the ultimate axial load increased significantly by increasing the concrete compressive strength or by decreasing the hollow ratio. However, increasing the inner-to-outer thicknesses ratio or the yield strength of the inner steel tube did not significantly increase the ultimate axial load. Chang et al. [8] and Wang et al. [9] studied the strength and ductility of CFT columns with steel sections and concluded that those types of columns have very high ductility and energy absorption capacities due to the composite action among the steel tube, steel section, and the core concrete; however, their ultimate bearing capacities are approximately equivalent to the simple superpositions of steel sections and the CFT columns, with no additional confinement produced by steel sections. Chithira and Baskar [10] studied the strength behavior of CFT columns with and without shear connectors, who found that the shear connectors did not significantly increase the load capacities of CFT columns. Xiamuxi et al. [11,12] also proposed a reinforcing method by applying axial reinforcement inside the steel tube to improve its overall mechanical property; the results have shown that, although reinforced CFT has better performance than CFT, the axial reinforcement cannot deduce the buckling of CFT stub columns, and over arranged reinforcement may cause pre-failure of concrete.

Welding technology has been commonly used in steel structures. In practice, however, it is difficult to guarantee the quality of welding when the wall of large diameter CFT column is too thick (e.g. thickness larger than 800 mm). Therefore, using relatively thin steel tube combined with welded stirrups on the steel tube could be an alternative method. Ding [1] studied square stirrup-confined CFT stub columns with cross ties, spiral, and rhombus stirrups. The results showed that welding bidirectional stirrups to the inner surface of the steel tube is the most efficient way in reinforcing square CFT stub columns. This approach has been validated for track-shaped concrete-filled steel tubular stub columns [13] as well.

In this paper, the reinforcing methods using stirrups were studied for circular CFT columns, thanks to the promising improvement on the mechanical properties of other sectional shapes of CFT columns. The main objectives and research scopes of this study are: (1) circular CFT stub columns with bidirectional stirrups, loop stirrups or orthogonal stirrups with the same volume-stirrup ratio were tested to investigate the effect of different stirrups forms on the overall ultimate bearing capacities and ductility; (2) circular loop stirrup-confined CFT stub columns with different volume-stirrup ratios were tested to investigate the effect of different volume-stirrup ratios on their ultimate bearing capacities and ductility; (3) 3D finite element modelling was established using ABAQUS for carrying out parametric studies; the confinement effect on the core concrete between stirrups and the steel tube were compared; (4) a simplified approach was developed to predict the ultimate bearing capacity of a stirrup-confined circular CFT stub column.

2. Experimental investigation

2.1. Specimens and material

A total of 5 groups of test specimens were designed, and the cross-sections of specimens are shown in Fig. 1. Geometric properties and characteristics of specimens are shown in Table 1, where the first number in the specimen label represents the type of stirrups: 1 for orthogonal stirrups; 2 for bidirectional stirrups; and 3 for loop stirrups. The CFT represents concrete-filled steel tubular stub column. The second number in the specimen label stands for the volume-stirrup ratio. Each test is repeated twice (namely A and B), therefore ten specimens were tested in total. The nominal dimensions of each specimen were 500 (D) mm × 4 (t) mm × 6(8/10) (d) mm × 1200 (H) mm. D is the diameter of the circular section; t is the wall thickness of the steel tube; H is the height of the specimen; d is the stirrups diameter; s is the spacing of longitudinal stirrups; ρ_s is the cross-sectional steel ratio; f_{cu} is the cubic compressive strength of the core concrete; f_s is the yield strength of the steel tube; f_{sv} is the yield strength of stirrups; $N_{u,e}$ is the experimental ultimate load-bearing capacity of a stub column; $N_{u,c}$ is the FE numerical ultimate load-bearing capacity of a stub column; DI is the ductility

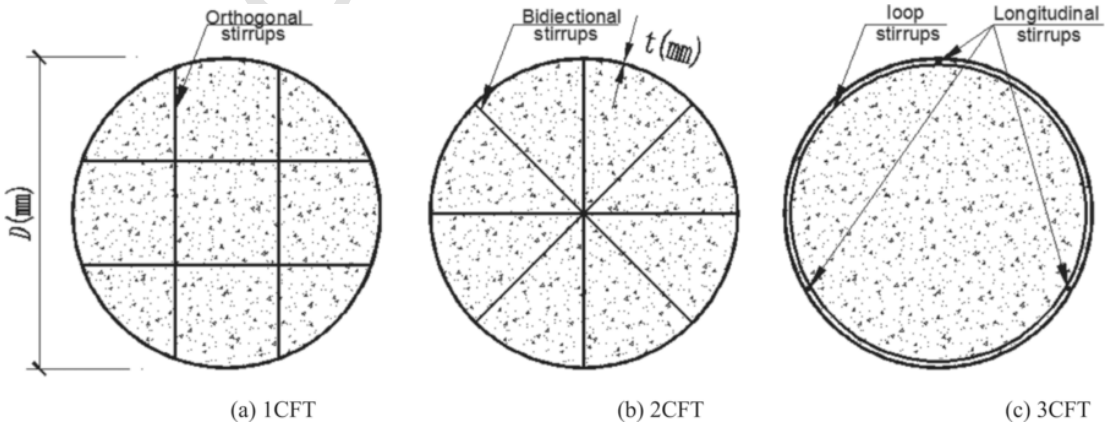

Fig. 1. Cross-sections of specimens.

Table 1
Properties of specimens.

Specimens label	$D \times t \times d \times H$/mm	s/mm	ρ_s /%	ρ_{sv} /%	ρ_{sa} /%	f_{cu} /MPa	f_s /MPa	f_{sv} /MPa	$N_{u,e}$ /kN	$N_{u,fe}$ /kN	$N_{u,3}$ /kN	DI	ρ_{sa}/ρ_s
1CFT1-A	500 × 3.65 × 5.98 × 1200	60	2.90	0.46	0.77	48.5	380	635	12,964	12,214	11,718	4.37	0.27
1CFT1-B	500 × 3.65 × 5.98 × 1200		2.90	0.46	0.77				12,304	12,214	11,718	4.45	0.27
2CFT1-A	500 × 3.77 × 6.03 × 1200	63	2.99	0.48	0.80				12,763	12,328	11,864	4.40	0.28
2CFT1-B	500 × 3.77 × 6.03 × 1200		2.99	0.48	0.80	12,288				12,328	11,868	3.78	0.28
3CFT1-A	499 × 3.70 × 5.80 × 1200	50	2.94	0.42	0.70				13,098	12,159	11,630	3.34	0.24
3CFT1-B	500 × 3.67 × 5.80 × 1200		2.91	0.42	0.70	11,700				12,103	11,641	2.09	0.24
3CFT2-A	500 × 3.70 × 7.58 × 1200	50	2.94	0.72	1.20				13,230	12,969	12,311	5.38	0.41
3CFT2-B	500 × 3.70 × 7.58 × 1200		2.94	0.72	1.20	13,043				12,969	12,311	5.16	0.41
3CFT3-A	500 × 3.70 × 8.82 × 1200	50	2.94	0.98	1.64				13,504	13,641	12,870	7.16	0.57
3CFT3-B	500 × 3.70 × 8.82 × 1200		2.94	0.98	1.64	13,434				13,641	12,870	7.05	0.57
c16-000	158 × 1.50 × 0 × 450	/	3.76	/	/		308	/	815	/	739	/	/
c23-000	158 × 2.14 × 0 × 450	/	5.34	/	/		286	/	907	/	857	/	/

index of a specimen; ρ_{sv} is the volume-stirrup ratio; ρ_{sa} is the equivalent stirrup ratio ($\rho_{sa} = \rho_{sv} \times f_{sv}/f_s$).

The volume-stirrup ratio of a circular CFT stub column with different types of stirrups can be calculated by the following equations:

$$\text{Orthogonal stirrups}: \quad \rho_{sv} = \frac{8\left(\frac{d}{2}\right)^2 \pi \sqrt{\left(\frac{D}{2}\right)^2 - \left(\frac{D}{6}\right)^2}}{\left(\frac{D}{2}\right)^2 \pi s} = \frac{8\sqrt{2}d^2}{3sD} \tag{1}$$

$$\text{Bidirectional stirrups}: \quad \rho_{sv} = \frac{4\left(\frac{d}{2}\right)^2 D\pi}{\left(\frac{D}{2}\right)^2 \pi s} = \frac{4d^2}{sD} \tag{2}$$

$$\text{Loop stirrups}: \quad \rho_{sv} = \frac{\left(\frac{d}{2}\right)^2 D\pi^2}{\left(\frac{D}{2}\right)^2 \pi s} = \frac{\pi d^2}{sD} \tag{3}$$

Each bidirectional (or orthogonal) stirrup was bent 90 degrees at both sides by 5 cm, then the bent parts were welded on the inner wall of the steel tube, as shown in Fig. 2(a). For the CFT stub column with loop stirrups, three longitudinal stirrups (diameters of 6 mm) were welded in the steel tube first, then the loop stirrups were welded to the longitudinal stirrups. All welding of stirrups began from the middle height and worked towards both ends of the steel tube. Fig. 2(b) shows circular steel tubes with different stirrups being tested.

Note that the method proposed in this paper mainly aims to solve the weldability and construction concerns for large-diameter CFT columns, i.e. diameter larger than 800 mm. This type of columns is commonly used for bridge piers, ground floor columns of ultra-high-rise buildings, large-scale shopping malls, and underground car parks. Welders can usually access those columns and do the welding either in-situ or off-site. The welding procedure used by the authors in lab is recommended for those large-scale columns. However, for a medium size CFT column, where it sees beneficial in using those types of stirrups, the authors would propose to make a reinforcement cage by pre-welding stirrups with longitudinal reinforcement bars, place the reinforcement cage in the steel tube, and weld the cage to the steel tube as much as possible.

2.2. Experimental set-up and measurements

Material properties of concrete and steel were tested before investigating the mechanical performance of the stirrup-confined circular CFT stub columns. Concrete standard cubes were tested according to Chinese standard GB/T50081-2002 [14] to investigate the cubic compressive strength of concrete. Tensile coupon tests according to Chinese standard GB/T228-2002 [15] were carried out using steel plates with

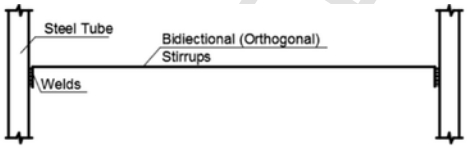

(a) Welding method of bidirectional (orthogonal) stirrups

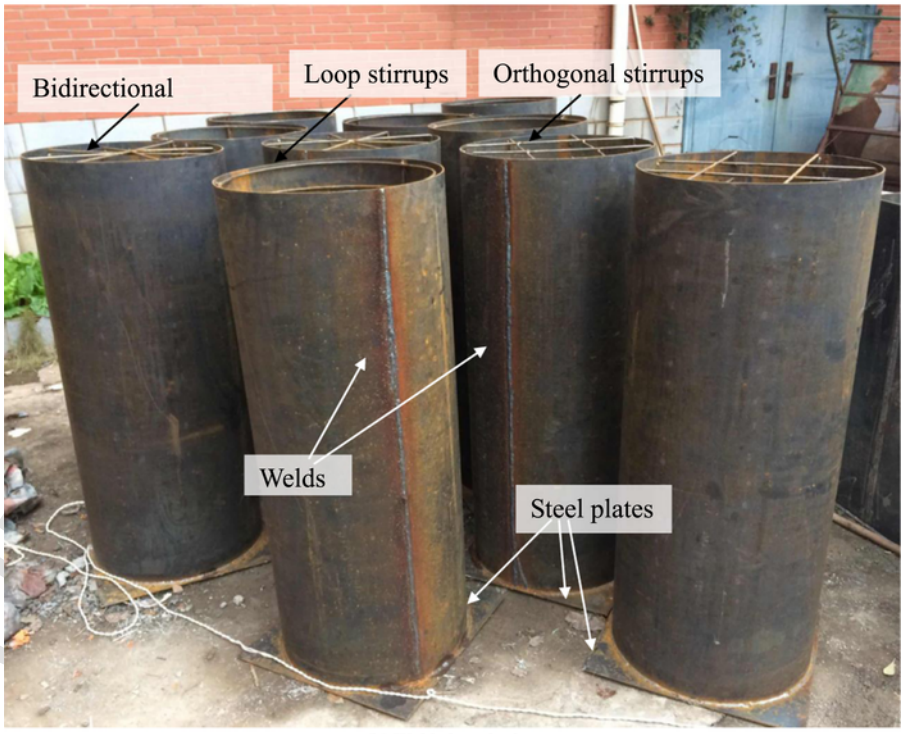

(b) Welded steel tubes

Fig. 2. Steel tubes with various stirrups.

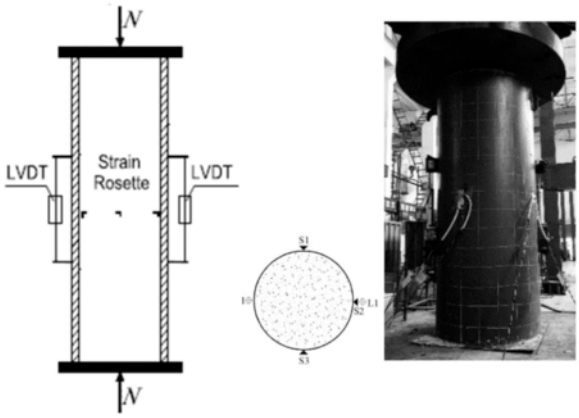

Fig. 3. Experimental instrumentation for all specimens.

thickness of 4 mm and stirrups with diameters of 6 mm, 8 mm and 10 mm. The tested material properties of concrete, steel and stirrups have been summarized in Table 1. (two paragraphs are missed) (next paragraph) Compressive experiments on stub column specimens were conducted using a 2000-ton tri-axial stress testing machine in the National Engineering Laboratory of Central South University. To accurately measure the deformation, three strain rosettes (S1 to S3) were attached at the mid-height and two LVDTs (L1 and L2) were installed at the same height of another two oppositeside surfaces, as shown in Fig.3. (next paragraph) The load is increased at a step of 1/10 of the expected ultimate load in the elastic stage and at a step of 1/20 of the expected ultimate load in the elastic–plastic stage. Each loading step takes 3-5 mins which is similar to a slow continuous loading mode and data is acquired by different classifications. When the ultimate load is approached, specimens are loaded slowly and continuously until failure and the data is recorded continuously. The loading of each specimen lasts about 1.5 h.

2.3. Test observations and failure modes

At the initial loading stage, all specimens showed elastic behavior as seen from the load-axial strain curves. The compressive stiffness of the specimen in this stage was larger than that in the other stages, and the axially elastic displacement of specimens and axial and transverse strain of steel tube were relatively small.

When the load increased to about 70% of the ultimate load, all specimens went into elastic-plastic stage, where local buckling of the steel tube occurred near both ends of the specimen due to the end effect. When the axial load reached the ultimate loading capacity, local buckling also occurred near the middle of the steel tube, although the increases of buckling deformations of 1CFT1 and 2CFT1 at the failure stage were not as significant as that of 3CFT1.

After the load reached the ultimate value, the bearing capacity was gradually decreased while the axial strain was continuously increased. The internal stirrup was snapped accompanied with crisp sound, and the buckling deformation of the steel tube became more obvious. The specimen began to show shear failure mode, and the experiment finally terminated due to excessive deformation. The load-axial strain relationship of stub columns is shown in Fig. 4. Typical failure modes of the stub columns were found to be local buckling at middle height and top end of specimens, and shear failure from the upper part to the lower part.

After experiments, the steel tubes were cut open in order to examine the failure mode of the core concrete. Inclined shear rupture zones were clearly seen from upper to lower parts of the core concrete. It was found that there was no weld failure of the spot welds between stirrups and the steel tube, and the stirrups did not affect the failure mode of the core concrete in the circular CFT columns. Typical failure modes of the stirrups-confined CFT specimens are shown in Fig. 5(a)–(d), while the failure mode of an ordinary circular CFT stub column adopted from literature [16] is shown in Fig. 5(e). The parameters of the specimens are shown in Table 1. All of the observed failure modes of the specimens were local buckling from the top to the middle portion as shown in Fig. 1. The shear failure zones of the stirrups-confined circular CFT stub columns were close to the middle positions, and the amplitudes were much smaller than that of ordinary circular CFT stub columns. It can be seen that stirrups can effectively reduce the local buckling of a CFT stub column.

2.4. Experimental results and discussion

Ultimate bearing capacities, ductility and Poisson's ratios of all 5 groups of stub columns have been plotted in Fig. 6 to Fig. 8, and the effects of different types of stirrups and volume-stirrup ratios will be discussed below.

2.4.1. Ultimate bearing capacity

(1) **Effect of the form of stirrups.** Fig. 6(a) shows that, with the same cross-sectional steel ratio of 2.9% and volume-stirrup ratio of 0.45%, the ultimate bearing capacities of three stub columns were close, although the ultimate bearing capacities of specimens 1CFT1 were the largest, followed by specimens 2CFT1. The average ultimate bearing capacity of specimens 1CFT1 was 0.86% higher than that of specimens 2CFT1, and 1.90% higher than that of specimens 3CFT1.
(2) **Effect of the volume-stirrup ratio.** The ultimate bearing capacities of specimens 3CFT are shown in Fig. 6(b). The average ultimate bearing capacity of specimens 3CFT2 was 5.95% higher than that of specimens 3CFT1 with an increase of 0.5% in the volume-stirrup ratio. For specimens 3CFT3, the average ultimate bearing capacity was 2.53% higher than that of specimens 3CFT2, while the volume-stirrup ratio was 0.44% higher. It is indicated that increasing the volume-stirrup ratio can effectively improve the bearing capacity of a stirrup-confined circular CFT stub column.

2.4.2. Ductility

To investigate the influence of various parameters on the ductility of specimens, the ductility index (*DI*) has been calculated using literature [17]:

$$DI = \frac{\varepsilon_{0.85}}{\varepsilon_{\mathrm{b}}} \tag{4}$$

where $\varepsilon_{0.85}$ is the axial strain when the load falls to 85% of the ultimate bearing capacity after the peak load; $\varepsilon_{\mathrm{b}} = \varepsilon_{0.75}/0.75$, where $\varepsilon_{0.75}$ is the axial strain under a load of 75% of the ultimate bearing capacity in the pre-peak stage. A higher *DI* value indicates a slower decrease of load after the ultimate state, thereby corresponding to a better ductile performance.

(1) **Effect of the form of stirrups.** The ductility indexes (*DI*) of 1CFT1, 2CFT1 and 3CFT1 are shown in Fig. 7(a). The *DI* of specimens 1CFT1 was 7.8% higher than specimens 2CFT1 and 62.4% higher than specimens 3CFT1. It is therefore indicated that, among the three stirrup forms, orthogonal stirrup performs best in increasing the constraint effect of the steel tube on the core concrete.
(2) **Effect of the volume stirrup ratio.** The ductility indexes of all specimen 3CFTs are shown in Fig. 7(b). Among them the specimens 3CFT3 demonstrated the highest *DI* value. Therefore, increasing the volume-stirrup ratio can efficiently increase the ductility of a CFT stub column.

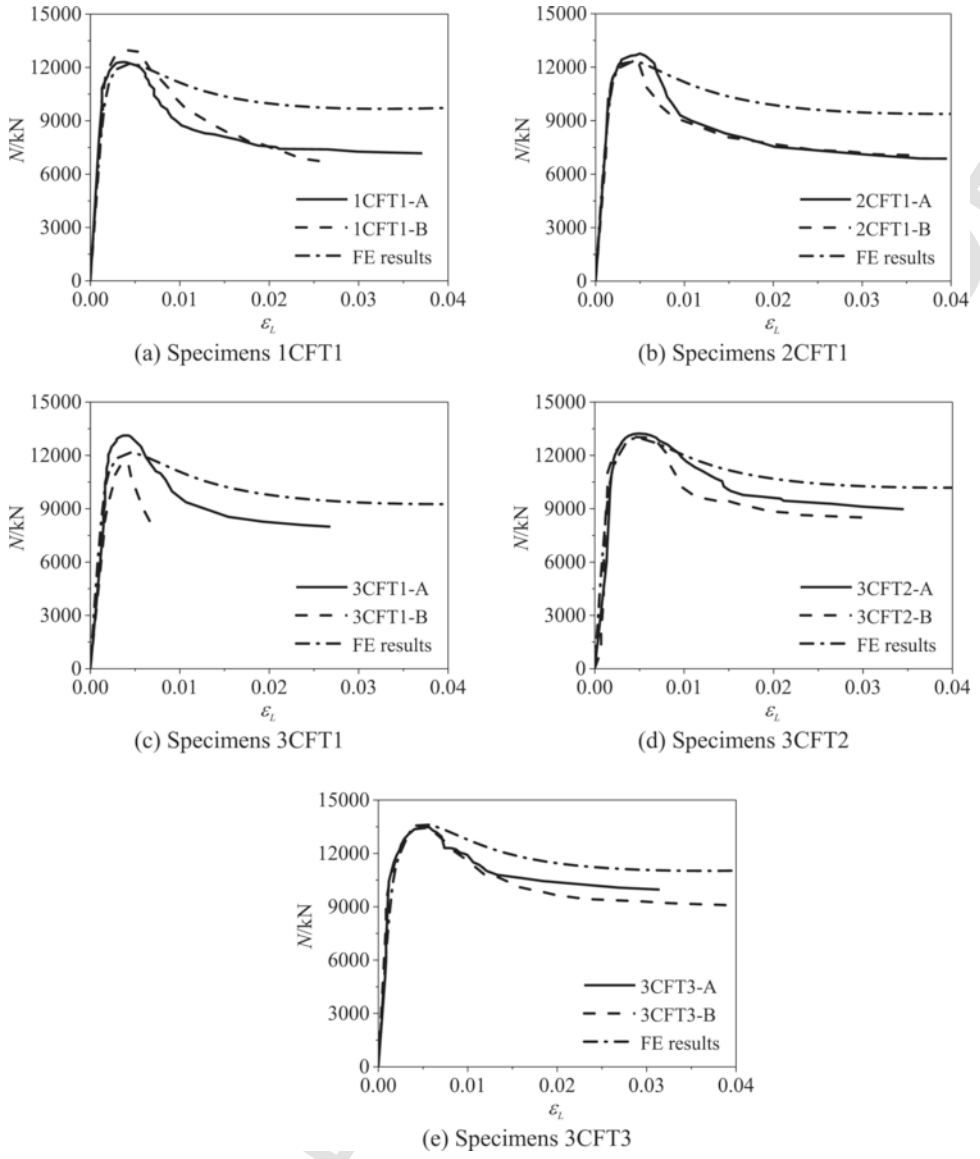

Fig. 4. Load-axial strain curves of stub columns under axially loading.

2.4.3. Poisson's ratio

The Poisson's ratio is defined as the absolute value of the perimeter strain divided by the axial strain. The average values of all gauges on the specimen were used for the axial and the lateral strain respectively. According to Yu et al. [18], an increase in the Poisson's ratio indicates increased confinement effect of the concrete core offered by the steel tube. Karimi et al. [19] and Ding et al. [1] stated that the Poisson's ratio is an important parameter for evaluating confinement effectiveness. The core concrete continually expands under loading, and the steel tube and stirrups constrain the expansion of the concrete due to confinement effect. On the other hand, stresses in the steel tube are highly affected by the state of the core concrete. The perimeter strain of the steel tube increases with the expansion of the core concrete, which leads to the increase of the Poisson's ratio of the steel tube. The higher the Poisson's ratio, the higher the composite action. The load- Poisson's ratio (v_{sc}) curves of 1CFT, 2CFT and 3CFT stub columns have been plotted in Fig. 8.

At the initial loading stage (the bearing capacity was less than 40% of the ultimate bearing capacity), the Poisson's ratio remained identical, which is close to the Poisson ratio of the steel. After then the Poisson's ratio increased slowly until the bearing capacity reached 80% of the ultimate bearing capacity, indicating that there was only minor composite action among the steel tube stirrups and the core concrete. When the specimen exceeded 80% of the ultimate bearing capacity, the Poisson's ratio began to increase rapidly. It continually increased after the ultimate bearing capacity was reached and even exceeded 1.0, which indicated that the steel tube produced significant constraint on the core concrete at this stage.

(1) **Effect of the form of stirrups.** Fig. 8(a) shows that with the increase of axial pressure, the Poisson's ratios of 1CFT1 and 2CFT1 stub columns were close and both increased faster than that of 3CFT1 stub column. It is indicated that the stirrups in 1CFT1 and 2CFT1 stub columns have stronger confinement effect on the core concrete than that of 3CFT1.

(2) **Effect of volume-stirrup ratio.** Fig. 8(b) shows the axial load versus Poisson's ratio curves of 3CFT specimens. At the initial loading stage, the average Poisson's ratio of 3CFT3 stub columns was larger than those of 3CFT1 and 3CFT2 stub columns. Therefore, the constraint effect of stirrups on the core concrete is improved with the increase of volume-stirrup ratio.

a) Local buckling at the top

(b) Shear failure

(c) Local buckling at the middle

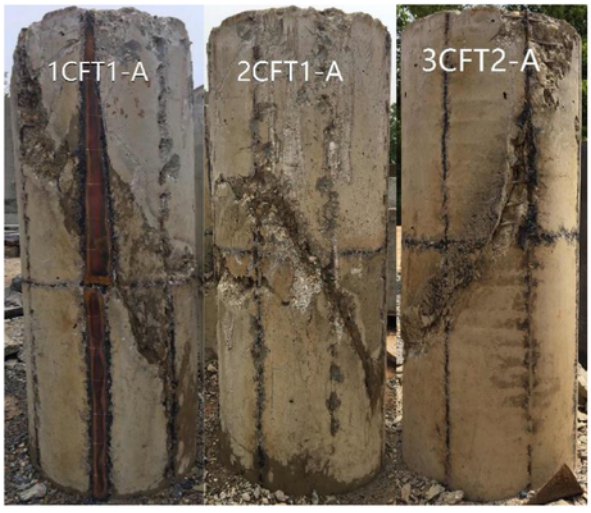

(d) Failure mode of the core concrete

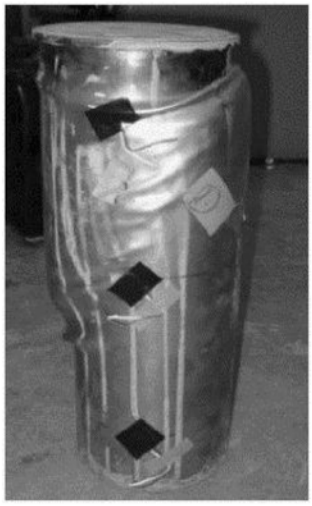

(e) Failure mode of circular CFT stub columns [16]

Fig. 5. Typical failure modes of specimens.

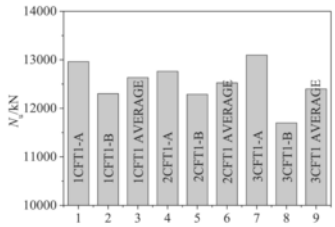

(a) Influence of stirrup forms on the ultimate bearing capacity

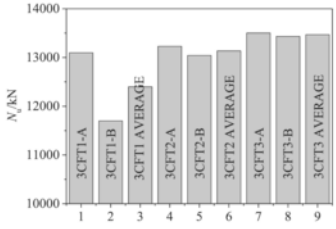

(b) Influence of volume-stirrup ratio on the ultimate bearing capacity

Fig. 6. Comparison of ultimate bearing capacities for all specimens.

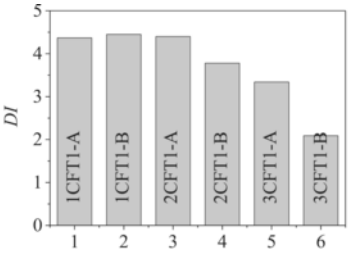

(a) Influence of stirrup forms on ductility index

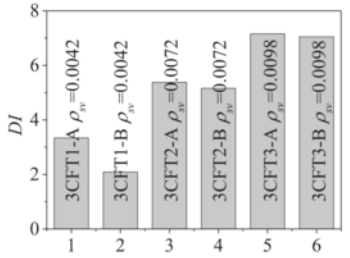

(b) Influence of volume-stirrup ratio on ductility index

Fig. 7. Comparison of ductility indexes for all specimens.

3. FE modelling

3.1. FE models

Nonlinear finite element (FE) analysis was carried out using commercial software ABAQUS/Standard 6.14 for investigating mechanical performance of stirrup-confined circular CFT stub columns under axial loading. 3D solid element (C3D8R) were used for the circular steel tube, the core concrete and the loading plate; 3D truss elements (T3D2) were used for the internal stirrups; and rigid elements were adopted for the loading plate to eliminate its deformation in the FE analysis.

A surface-to-surface contact was adopted for the constraint between the steel tube and the core concrete with finite slip formula. The interaction of the normal direction of two surfaces was hard contact. In the tangential direction, a friction coefficient of 0.5 was used in the analysis. A tie constraint was adopted between the loading plate and the CFT column so that no relative motion was allowed. Stirrups were embedded in core concrete at specified positions. The FE model is shown in Fig. 9.

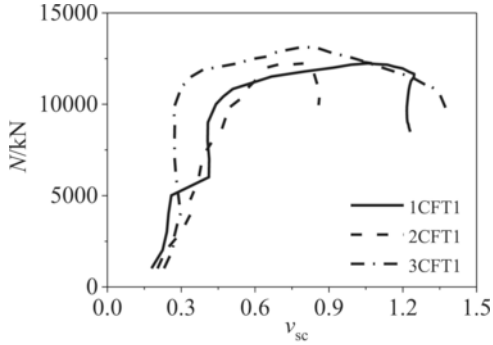

(a) 1CFT1, 2CFT1 and 3CFT1

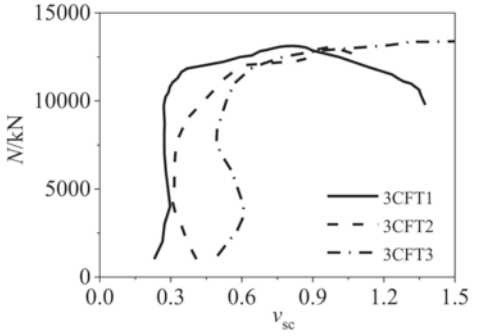

(b) 3CFT1, 3CFT2 and 3CFT3

Fig. 8. Axial load vs. Poisson's ratio curves of the steel tubes among 1CFT, 2CFT and 3CFT.

The tri-axial compression plasticity-damage constitutive model [21] was adopted for the core concrete of a stirrup-confined circular CFT stub column; a bilinear elasto-plastic model, associated with the Prandtl-Reuss flow rule, was used to describe the constitutive behavior of the steel tube and stirrups. The stress-strain relationship of the core concrete, the steel tube and the stirrups are described in literature [21]. The above constitutive models have been successfully applied in the track-shaped, square stirrup-confined CFT stub columns [1,13].

3.2. Model verification

The ultimate bearing capacities obtained from experiments and FEA are shown in Table 1. The FE results agreed well with experiments, with an average error of 1.4% and a coefficient of dispersion of 0.045. The load-axial stain curves of all specimens obtained from both FE modelling and experiment have been shown in Fig. 4. Good agreement has been achieved between experimental and FE modelling results in the elastic stage. However, larger deviations have occurred in the elastic-plastic stage and failure stage. FE models have been found to overpredict the post-yielding behavior compared with experimental results. Due to unavoidable defects in the steel tube and the non-homogeneous characteristics of concrete material, the core concrete and the steel tube were prone to uneven deformation under loading, which accelerated the local buckling of the steel tube and lead to rather rapid decline of the bearing capacity of the CFT stub column in the elastic-plastic stage and failure stage. However, due to the simplifications of the FE modelling, those characteristics could not be captured in the numerical analysis.

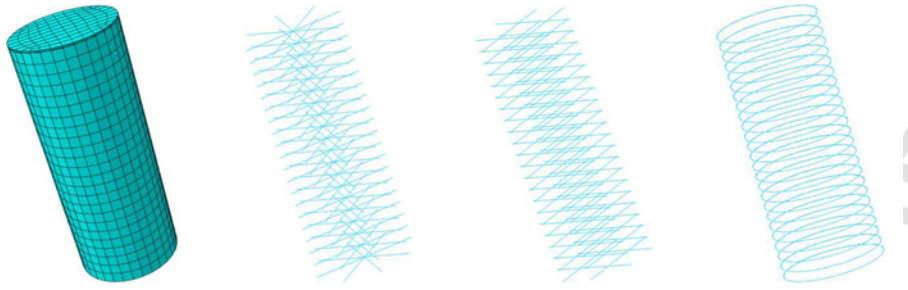

Fig. 9. Mesh generation of FE models.

3.3. Composite action analysis

The validated FE model was then used to investigate the composite action among core concrete, steel tube and stirrups of a stirrup-confined circular CFT stub column, and the results have been shown in Fig. 10:

1) Fig. 10(a) shows the relationship of stirrups stress versus axial strain at the mid-heights of specimens. The stirrups have reached yielding in all three types of stirrup-confined circular CFT stub columns. Overall the orthogonal stirrups showed largest confinement on the core concrete, followed by bidirectional stirrups and loop stirrups.
2) Fig. 10(b) shows the axial stress-strain curves and transverse stress-strain curves of the steel tubes at the mid height. It is found that the intersection appeared earliest in the specimen with orthogonal stirrups, followed by the ones with bidirectional stirrups and loop stirrups. When the CFT column was axially loaded, both the concrete and the steel tube were compressed until the axial yield strain was reached. After then the core concrete expanded increasingly under loading, which led to increasing transverse stress in the steel tube due to confinement. According to the Mises yield criterion [20], the axial stress of the steel tube decreased with the increase of the transverse stress. Therefore, the earlier the intersection appeared, the stronger the composite action was. It is again illustrated that the composite action of the circular CFT stub column with orthogonal stirrups is the greatest among all three types of stirrups-confined circular CFT columns.
3) Fig. 10(c) plots the average axial stress-strain curves of the core concrete. The circular CFT stub column with orthogonal stirrups showed highest axial stress among all circular CFT stub columns, with or without stirrups.

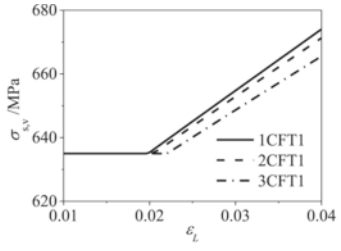

(a) Stirrup average stress of 1CFT1, 2CFT1 and 3CFT1

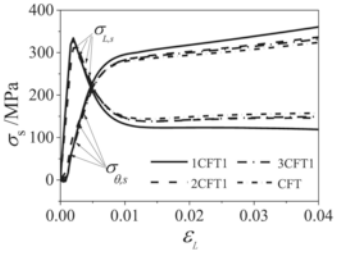

(b) Steel stress-strain relationships from calculated results

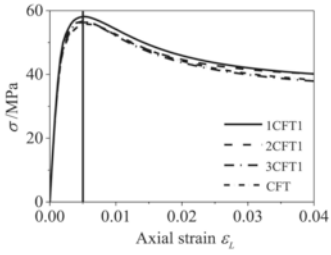

(c) Axial stress-axial strain relationship of core concrete

Fig. 10. Stress-axial strain curves among specimens 1CFT1, 2CFT1 and 3CFT1 from FE results.

The axial ultimate bearing capacities of circular CFT stub columns, with and without orthogonal stirrups, have been summarized in Table 2. The same overall steel ratio (i.e., transferring the volume of stirrups to the steel tube) and same core concrete cross-sectional area have been adopted. It was found that the ultimate bearing capacity of a circular CFT stub column with orthogonal stirrups was slightly higher than that of a circular CFT stub column with no stirrups. Therefore, using orthogonal stirrups could be an alternative reinforcing method in large diameter circular CFT stub columns, in order to satisfy an overall steel ratio while ensuring weldability of steel tubes.

3.4. Comparison of confinement effects

Radial stress of the core concrete ($\sigma_{r,c}$),which reflects confinement effects of stirrups and the steel tube on the core concrete, can be expressed as:

$$\sigma_{r,c} = \sigma_{r,c1} + \sigma_{r,c2} \tag{5}$$

where $\sigma_{r,c1}$ is radial stress of the core concrete caused by the steel tube, and $\sigma_{r,c2}$ is radial stress of the core concrete caused by stirrups. According to Ding et al. [20],

$$\sigma_{r,c1} = \frac{\rho_s}{2(1-\rho_s)}\sigma_{\theta,s} \tag{6}$$

where $\sigma_{\theta,s}$ is the tensile transverse stress of the steel tube.

Substituting Eq. (6) into Eq. (5), radial stress of the core concrete caused by stirrups can be described as:

$$\sigma_{r,c2} = \sigma_{r,c} - \frac{\rho_s}{2(1-\rho_s)}\sigma_{\theta,s} \tag{7}$$

Table 2
Comparisons of ultimate bearing capacities of FE models between CFT and 1CFT with same steel ratios.

Overall steel ratio	D /mm	f_s /MPa	f_{sv} /MPa	f_{cu} /MPa	CFT	1CFT				CFT	1CFT	Increased value
					t/mm	ρ_s	t/mm	ρ_{sv}	d/mm	$N_{u,ef}$/kN	$N_{u,ef}$/kN	
0.045	500	380	635	48.5	5.69	0.04	5.05	0.005	4.82	12,944	13,059	0.8%
0.05					6.33			0.01	6.81	13,523	13,714	1.4%
0.055					6.97			0.015	8.35	14,107	14,335	1.6%
0.06					7.62			0.02	9.64	14,703	14,919	1.5%

$\sigma_{r,c1}$ and $\sigma_{r,c2}$ obtained from FEA and Eq. (7) are shown in Fig. 11. It is found that $\sigma_{r,c1}$ and $\sigma_{r,c2}$ increased with the increase of axial strain before the specimens reached their ultimate bearing capacities. After the ultimate state, $\sigma_{r,c2}$ gradually decreased, while $\sigma_{r,c1}$ continually increased. The $\sigma_{r,c1}$ and $\sigma_{r,c2}$ of the ultimate state are shown in Table 3. With the increase of volume-stirrups ratio, $\sigma_{r,c2}$ is increased more significantly than $\sigma_{r,c1}$. When the equivalent stirrup ratio is 1.64% (specimen 3CFT3), $\sigma_{r,c2}$ even exceeds $\sigma_{r,c1}$ at the ultimate state. It can be seen that stirrups can effectively restrain the core concrete, and their confinement effect could be even greater than that of the steel tube on the core concrete.

4. Bearing capacity calculation

4.1. Model simplifications

Parametric studies were carried out in this paper for investigating the mechanical performance of stirrup-confined circular CFT stub columns. A total of 72 models were performed covering the following parameters: nominal steel yield strength f_s ranged from Q235 to Q420; concrete strength f_{cu} ranged from C40 to C100; diameter (D) was 500 mm; length (L) was 2D; the cross-sectional steel ratios ρ_s were 0.05 and 0.08 respectively; and the equivalent stirrup ratios were 0.005 and 0.01 respectively. The following steel and concrete were paired up in the parametric studies: C40 concrete was paired with Q235 steel; C60 concrete was paired with Q235 and Q345 steel; C80 concrete was paired with Q345 and Q420 steel; and C100 concrete was paired with Q420 steel. The ratios of axial compressive stresses ($\sigma_{L,s}$) to the yield strength (f_s) ($f_{sc} = N_u/A_{sc}$, where $A_{sc} = A_c + A_s$ is the total cross-section area) of the steel tubes in the middle sections at the ultimate state have been obtained, as shown in Fig. 12. The average ratio of the axial compressive stress to the yield stress of a steel tube at the ultimate state could be expressed as:

$$\sigma_{L,s} = 0.69 f_s \tag{8}$$

Based on von Mises yield criterion [20], the tensile transverse stress ($\sigma_{\theta,s}$) of a steel tube can be obtained as:

$$\sigma_{\theta,s} = 0.59 f_s \tag{9}$$

Fig. 13 plots the von Mises stress contours at the ultimate states of the circular CFT stub columns, with and without stirrup confinement. It is found that the confining effect of the circular steel tube and stirrups on the core concrete is evenly distributed. The average axial stress of the core concrete in a stirrup-confined circular CFT stub column is higher than that of the ordinary circular CFT stub column.

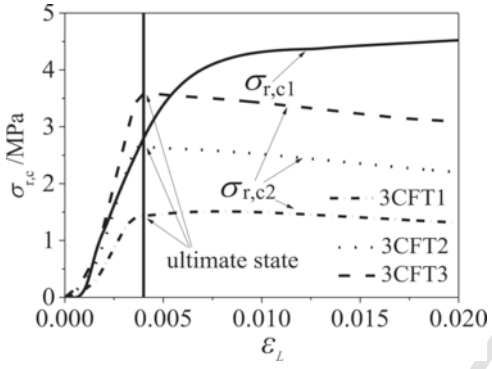

Fig. 11. Radial stress of the core concrete caused by the steel tube ($\sigma_{r,c1}$) and stirrups ($\sigma_{r,c2}$).

Table 3
The $\sigma_{r,c1}$ and $\sigma_{r,c2}$ at the ultimate state.

	ρ_s/%	ρ_{sa}/%	$\sigma_{r,c1}$/MPa	$\sigma_{r,c2}$/MPa
3CFT1	2.9	0.7	3.07	1.45
3CFT2	2.9	1.2	3.11	2.63
3CFT3	2.9	1.64	3.22	3.56

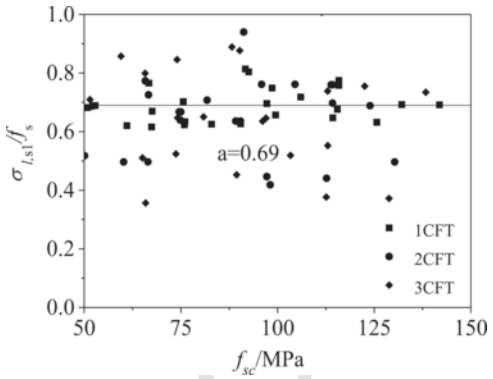

Fig. 12. Average ratios of axial compressive stresses to yield stresses of the steel tubes.

4.2. Simplified calculation method

The stress distribution of a stirrup-confined circular CFT stub column can be simplified as shown in Fig. 14. To facilitate design, stirrups are transformed into the circular steel tube using an equivalent wall thickness, in order to match the steel ratio. The sectional area of the equivalent steel tube A_{sso} for a circular CFT stub column with orthogo-

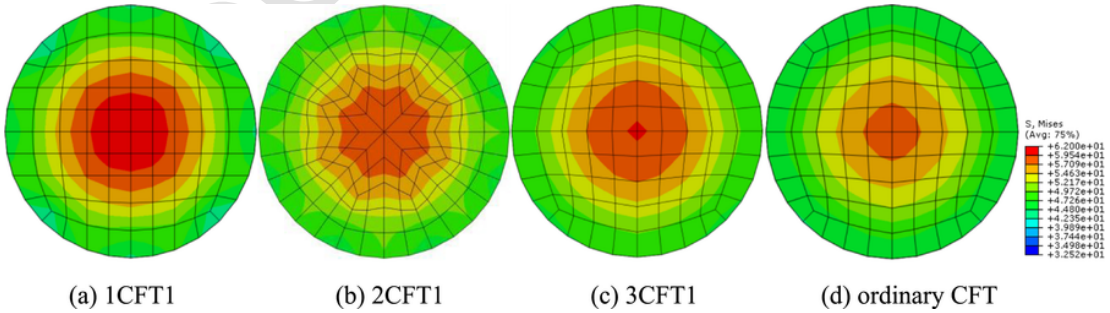

Fig. 13. Stress contours at mid-sections for circular CFT stub columns with and without stirrups.

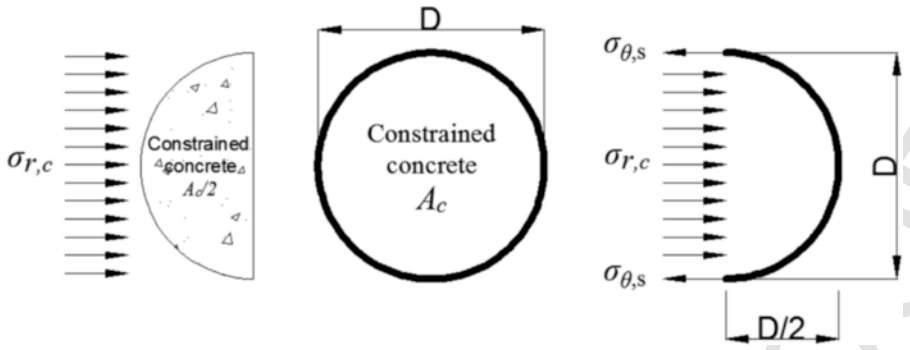

Fig. 14. Simplified stress distribution within the mid-section of a stirrup-confined circular CFT stub column.

nal stirrups can thereby be calculated by the following equation:

$$A_{sso} = \frac{\frac{d^2}{4}\pi \times 8\sqrt{(\frac{1}{2}(D-2t))^2 - (\frac{1}{6}(D-2t))^2}}{s} = \frac{2\sqrt{2}(D-2t)d^2\pi}{3s} \quad (10)$$

The sectional area A_{sso} for a circular CFT stub column with bidirectional stirrups can be calculated by Eq. (11):

$$A_{sso} = \frac{(D-2t)d^2\pi}{s} \quad (11)$$

and the sectional area A_{sso} for a circular CFT stub column with loop stirrups can be calculated by:

$$A_{sso} = \frac{(D-2t)d^2\pi^2}{4s} \quad (12)$$

From Fig. 13, the following relationship yields

$$\sigma_{r,c} = \frac{f_{sv}A_{sso}}{2A_c} + \frac{\rho_s}{2(1-\rho_s)}\sigma_{\theta,s} \quad (13)$$

The longitudinal compressive stress of the core concrete ($\sigma_{L,c}$) can be expressed as:

$$\sigma_{L,c} = f_c + k\sigma_{r,c} \quad (14)$$

in which k (=3.4) is the lateral pressure coefficient adopted from literature [20].

According to the static equilibrium of the cross-section, the ultimate bearing capacity $N_{u,3}$ of an axially-loaded stirrup-confined circular CFT stub columns can be expressed as:

$$N_{u,3} = \sigma_{L,c}A_c + \sigma_{L,s}A_s \quad (15)$$

Substituting Eqs. (8)–(14) into Eq. (15), the axial-loading bearing capacity of a stirrup-confined circular CFT stub column can be described as:

$$N_{u,3} = f_cA_c + 1.7f_sA_s + Pf_{sv}A_{sso} \quad (16)$$

where P is the coefficient for different types of stirrup-confined circular CFT stub columns. For the specimens 1CFT1, 2CFT1 and 3CFT1, the coefficients have been found to be 1.7032, 1.7005 and 1.6996, respectively. An identical value of $P = 1.7$ is thereby proposed. Eq. (16) can then be rewritten as:

$$N_{u,3} = f_cA_c + 1.7(f_sA_s + f_{sv}A_{sso}) \quad (17)$$

Fig. 15 shows the ultimate bearing capacities from experiments ($N_{u,e}$), Eq. (17) ($N_{u,3}$) and FE modelling ($N_{u,fe}$). The average ratio of $N_{u,e}$ to $N_{u,3}$ is 1.062 with a dispersion coefficient of 0.033, and the average ratio of $N_{u,fe}$ to $N_{u,3}$ is 1.048, with a dispersion coefficient of 0.008. Therefore, it is concluded that the proposed formula agrees well with experimental and FE results.

The ultimate bearing capacity of a circular CFT stub column with a steel section [8,9] or steel reinforcement [11,12] is usually described as a simple superposition of the steel section (or steel reinforcement) and the ordinary CFT column, without any additional confining effect produced by the steel section (or steel reinforcement). The steel section or steel reinforcement can only work up to its yield strength. However, the innovative reinforcement proposed in this paper can perform up to 1.7 times of its yield strength, which is equivalent to the confinement of the steel tube. It is then concluded that the constraint of the stirrup-confined forms is more effective than steel sections or steel reinforcement to circular CFT stub columns.

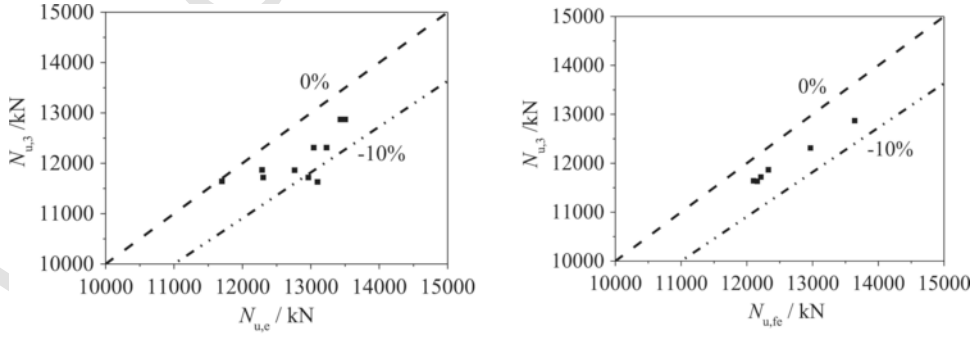

(a) Comparison of ultimate bearing capacities obtained from Eq. (17) and test results

(b) Comparison of ultimate bearing capacities obtained from Eq. (17) and FE results

Fig. 15. Comparison of ultimate bearing capacities among calculated results using Eq. (17), FE results and experimental results.

5. Conclusions

This paper presents a comparative study of circular CFT stub columns with three different stirrup-confined forms: orthogonal stirrups, bidirectional stirrups and loop stirrups. Based on the experimental and numerical results, the following conclusions can be drawn:

(1) The stirrups did not affect the failure modes of the circular CFT columns. All stirrup-confined circular CFT columns had local buckling failure in the steel tube at the middle height and the top end of a circular CFT column, and shear failure in the core concrete.
(2) The ultimate bearing capacity and ductility of a circular CFT stub column with orthogonal stirrups were higher than those of the other two stirrup types. Increasing the volume-stirrup ratio will increase the ultimate bearing capacity and ductility of a stirrup-confined circular CFT stub column significantly.
(3) The composite action increased with the increase of the volume-stirrup ratio. With the same volume-stirrup ratio, orthogonal stirrups produced strongest composite action among the three different types of stirrups. Moreover, radial stress of the core concrete resulted from stirrups was greater than that by the steel tube.
(4) A simplified design approach, validated by experimental and numerical results, was developed to predict the ultimate bearing capacity of a stirrup-confined circular CFT stub column. The confinement on the core concrete provided by stirrups investigated in this paper strongly outperformed that provided by steel sections or steel reinforcement in literatures.

Acknowledgments

This research work was financially supported by the National Natural Science Foundation of China, Grant no. 51578548.

References

[1] F.X. Ding, D.R. Lu, Y. Bai, Q.S. Zhou, M. Ni, Z.W. Yu, G.S. Jiang, Comparative study of square stirrup-confined concrete-filled steel tubular stub columns under axial loading, Thin-Walled Struct. 98 (2016) 443–453.
[2] Y. Lu, N. Li, S. Li, Behavior of FRP-confined concrete-filled steel tube columns, Polymer 6 (5) (2014) 1333–1349.
[3] J.G. Teng, Y.M. Hu, Y. Tao, Stress–strain model for concrete in FRP-confined steel tubular columns, Eng. Struct. 49 (2013) 156–167.
[4] Y.M. Hu, T. Yu, J.G. Teng, FRP-confined circular concrete-filled thin steel tubes under axial compression, J. Compos. Constr. 15 (5) (2011) 850–860.
[5] J.W. Park, Y.K. Hong, G.S. Hong, J.H. Kim, S.M. Choi, Design formulas of concrete filled circular steel tubes reinforced by carbon fiber reinforced plastic sheets, Proc. Eng. 14 (2011) 2916–2922.
[6] M.F. Hassanein, O.F. Kharoob, Q.Q. Liang, Circular concrete-filled double skin tubular short columns with external stainless steel tubes under axial compression, Thin-Walled Struct. 73 (2013) 252–263.
[7] M.F. Hassanein, O.F. Kharoob, L. Gardner, Behaviour and design of square concrete-filled double skin tubular columns with inner circular tubes, Eng. Struct. 100 (2015) 410–424.
[8] X. Chang, Y.Y. Wei, Y.C. Yun, Analysis of steel-reinforced concrete-filled-steel tubular (SRCFST) columns under cyclic loading, Constr. Build. Mater. 28 (1) (2012) 88–95.
[9] Q. Wang, D. Zhao, P. Guan, Experimental study on the strength and ductility of steel tubular columns filled with steel-reinforced concrete, Eng. Struct. 26 (7) (2004) 907–915.
[10] K. Chithira, K. Baskar, Experimental study on circular concrete filled steel tubes with and without shear connectors, Steel Compos. Struct. 16 (1) (2014) 99–116.
[11] A. Xiamuxi, A. Hasegawa, Experimental study on reinforcement ratio of RCFT columns under axial compression, Adv. Mater. Res. 250 (2011) 3790–3797.
[12] A. Xiamuxi, A. Hasegawa, A study on axial compressive behaviors of reinforced concrete filled tubular steel columns, J. Constr. Steel Res. 76 (2012) 144–154.
[13] F.X. Ding, L. Fu, X.M. Liu, J. Liu, Mechanical performances of track-shaped rebar stiffened concrete-filled steel tubular (SCFRT) stub columns under axial compression, Thin-Walled Struct. 99 (2016) 168–181.
[14] GB/T50081-2002 Strandard for Method of Mechanical Properties on Ordinary Concrete China Building Industry Press Beijing 2001
[15] GB/T228-2002 Metallic Materials-Tensile Testing at Ambient Temperatures Standards Press of China Beijing 2002
[16] Kojiro Uenaka, Hiroaki Kitoh, Keiichiro Sonoda, Concrete filled double skin circular stub columns under compression, Thin-Walled Struct. 48 (1) (2010) 19–24.
[17] L.H. Han, G.H. Yao, X.L. Zhao, Tests and calculations for hollow structural steel (HSS) stub columns filled with self-consolidating concrete (SCC), J. Constr. Steel Res. 61 (9) (2005) 1241–1269.
[18] Z.-W. Yu, F.-X. Ding, C.-S. Cai, Experimental behavior of circular concrete-filled steel tube stub columns, J. Constr. Steel Res. 63 (2) (2007) 165–174.
[19] J. Kian Karimi, W. Michael Tait, Wael EI-Dakhakhni Influence of slenderness on the behavior of a FRP-encased steel-concrete composite column, J. Compos. Constr. 16 (1) (2012) 100–109.
[20] F. Ding, Z. Yu, Y. Bai, Y. Gong, Elasto-plastic analysis of circular concrete-filled steel tube stub columns, J. Constr. Steel Res. 67 (10) (2011) 1567–1577.
[21] F. Ding, X. Ying, L. Zhou, Z. Yu, Unified calculation method and its application in determining the uniaxial mechanical properties of concrete, Front. Struct. Civ. Eng. 5 (3) (2011) 381–393.